Global and local phase-unwrapping techniques: a comparison

Gianfranco Fornaro

Istituto di Ricerca per l'Elettromagnetismo e i Componenti Elettronici, Consiglio Nazionale delle Ricerche, Via Diocleziano 328, 80124 Napoli, Italy

Giorgio Franceschetti

Dipartimento di Ingegneria Elettronica, Università di Napoli Federico II, Via Claudio 21, 80125 Napoli, Italy, and Department of Electrical Engineering, University of California, Los Angeles, 405 Hilgard Avenue, Los Angeles, California 90024-1600

Riccardo Lanari

Istituto di Ricerca per l'Elettromagnetismo e i Componenti Elettronici, Consiglio Nazionale delle Ricerche, Via Diocleziano 328, 80124 Napoli, Italy

Eugenio Sansosti

Istituto di Ricerca per l'Elettromagnetismo e i Componenti Elettronici, Consiglio Nazionale delle Ricerche, Via Diocleziano 328, 80124 Napoli, Italy

Manlio Tesauro

Dipartimento di Ingegneria Elettronica, Università di Napoli Federico II, Via Claudio 21, 80125 Napoli, Italy

Received January 10, 1997; revised manuscript received May 1, 1997; accepted May 6, 1997

We investigate the relationship between local and global phase-unwrapping techniques. We demonstrate that both algorithms are based on line integration of an estimate of the phase gradient: the former evaluates the integral along a single path, and the latter averages integrals along many paths. This analysis is extended to the weighted case. We also give an interpretation of the errors caused by an incorrect phase-gradient estimate in terms of path-following integrals.
[S0740-3232(97)03010-X]

1. INTRODUCTION

Two-dimensional phase unwrapping is a problem common to a wide variety of scientific and application areas; it denotes the retrieval of the original (unwrapped) phase ϕ starting from the corresponding restricted (wrapped) phase ϕ_m in the $(-\pi, \pi)$ interval. Recently this problem has been investigated extensively with respect to remote sensing because of its application to the generation of precise digital elevation models by means of interferometric synthetic-aperture radar.[1–3]

Most of the algorithms presented in the literature are based on two steps[4–15]: (1) generation of an estimate **s** of the unwrapped phase gradient starting from the wrapped data ϕ_m and (2) integration of the computed estimate **s**.

With respect to the first step, it has been widely pointed out[8–12] that if the unwrapped phase gradient, say, $\nabla\phi$, is less than π in magnitude, then it can be simply calculated by restricting the wrapped phase gradient, say, $\nabla\phi_m$, in the $(-\pi, \pi)$ interval. Thus we can express the estimated unwrapped phase gradient as $\mathbf{s} = \langle \nabla\phi_m \rangle$, where $\langle\ \rangle$ is the operator that restricts to the $(-\pi, \pi)$ interval (wrapping operator). Unfortunately, this constraint is usually not satisfied everywhere within the data. This happens in the areas, referred hereafter to as corrupted regions, where the unwrapped phase exhibits either an intrinsic high variation or a low signal-to-noise ratio. This problem is usually dealt with in the integration step, as we will see in the following.

The integration step can be performed in two different ways: (1) by local integration[4,13,14] or (2) by global integration.[5–12,15]

In the local-integration methods, the unwrapped phase is computed by integrating the estimated phase gradient **s** over a path that connects all the image points, starting from a fixed point P_0. The result can be written, as a generic point P, as follows:

$$\phi(\mathbf{r}) = \phi_0 + \int_{P_0}^{P(\mathbf{r})} \mathrm{d}c\, \mathbf{s}(\mathbf{r}) \cdot \hat{\mathbf{c}}, \qquad \phi_0 = \phi(P_0), \quad (1)$$

where $\hat{\mathbf{c}}$ is a unit vector along the integration path (Fig. 1). In absence of any corrupted region the integral in Eq. (1) is path independent because the vector field **s** equals the unwrapped phase gradient and thus is irrotational ($\nabla \times \mathbf{s} = 0$).

0740-3232/97/1002702-07$10.00

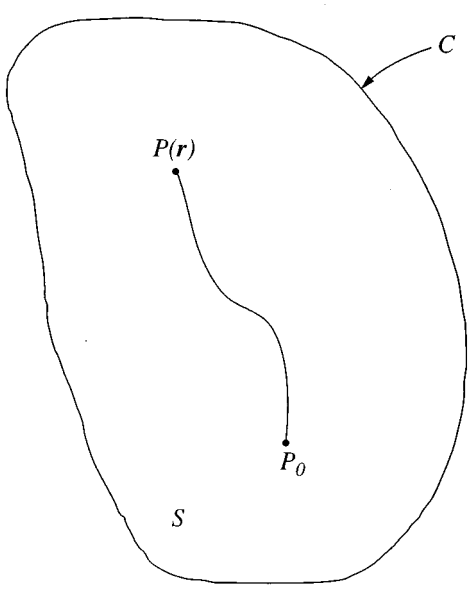

Fig. 1. Relevance of local integration.

In the presence of some residues, i.e., the points where $\nabla \times \mathbf{s} \neq 0$, the solution will be path dependent and no longer unique. Because $\mathbf{s}$ is a planar vector, $\nabla \times \mathbf{s}$ will be orthogonal to the $\mathbf{s}$ plane; depending on the orientation of $\nabla \times \mathbf{s}$, the residues are referred to as positive or negative. A well-known approach to avoiding the path dependence of the solution is based on inserting branch cuts (or cut lines) between residues of opposite polarity and preventing the integration path from crossing any of these cuts.[4] Since we can detect residue polarity and location only from the wrapped data, many cut lines are possible. Several efforts have been made to develop methods of cut-line generation.[13,16–20] If all the branch cuts are properly set there will be a unique (path-independent) solution to the problem of the phase unwrapping. However, a wrong choice even of a single branch cut might produce an error propagation.

The global integration algorithms perform a path-independent integration that is carried out again on the estimated phase gradient. The least-squares (LS) procedure presented in Refs. 5–9 is based on the minimization of the squared distance between the vector field $\mathbf{s}$ and the true gradient of the unknown unwrapped phase:

$$\|\mathbf{s} - \nabla\phi\|^2 = \min. \tag{2}$$

This phase-unwrapping method is amenable to numerical implementation. It has also been shown[10,12] that an alternative solution to Eq. (2) is provided by

$$\phi(\mathbf{r}') = -\iint_S \mathrm{d}S\,\mathbf{s}(\mathbf{r}) \cdot \nabla g(\mathbf{r}' - \mathbf{r}) + \oint_C \mathrm{d}c\,\phi(\mathbf{r}_C)\,\frac{\partial g(\mathbf{r}' - \mathbf{r}_C)}{\partial n}, \qquad \mathbf{r}' \in S, \tag{3}$$

where S is the (planar) domain under investigation, C is its boundary, and $g(\mathbf{r})$ is the Green's function for the unbounded domain[10]:

$$\nabla^2 g(\mathbf{r}) = \delta(\mathbf{r}). \tag{4}$$

The solution provided by Eq. (3), which was developed independently from the LS approach,[10] is referred to as the Green's function method and provides a direct answer to the global phase-unwrapping problem, once the phase on the boundary $\phi(\mathbf{r}_C)$ has been estimated. In Ref. 10 it was also shown that the required phase on the boundary can be estimated from the measured data by solving a Fredholm equation of the second kind.

In the presence of corrupted regions, the result obtained by global algorithms may exhibit errors, that are too great in some applications (that is, the case of synthetic aperture radar interferometry). Therefore the corrupted regions must be excluded from the integration by using weighting functions, as discussed in Refs. 5 and 8. Weighted global phase-unwrapping procedures require the explicit definition of the weighting function, which cannot be directly computed from the wrapped data: This is a problem similar to that of the selection of branch cuts in local algorithms.[15]

The relationship between local and global phase-unwrapping procedures is exploited in this study. In Section 2 we discuss the basic connection that exists between these procedures in the absence of any corrupted region. In Section 3 we extend the previous analysis to the periodic case, which is particularly relevant when rectangular domains are investigated. Section 4 is dedicated to demonstrating that the previously shown relationships are still valid in the weighted case. In Section 5 the effect of the nonexcluded corrupted regions on the unwrapped phase is analyzed in terms of path-following integrals.

2. BASIC CONNECTION BETWEEN GLOBAL AND LOCAL TECHNIQUES

Equation (1) provides a definite phase value $\phi(\mathbf{r})$ at any point P($\mathbf{r}$) by direct integration along a chosen path. In the LS method, Eq. (2), apparently there is no connection between the retrieved phase, $\phi(\mathbf{r})$, and integration paths, but this is not true. To explore this point we start from the LS solution in Eq. (3), wherein the Green's function is given by[10]

$$g(r) = \frac{1}{2\pi}\ln(1/r), \tag{5}$$

$$\nabla g(r) = -\frac{1}{2\pi}\frac{\hat{\mathbf{r}}}{r}. \tag{6}$$

We use polar coordinates for to evaluate Eq. (3), and we obtain

$$\phi(0) = \oint_C \mathrm{d}c\,\phi(r_M,\,\theta)\,\frac{\hat{\mathbf{r}}\cdot\hat{\mathbf{n}}}{2\pi r_M} - \int_0^{2\pi}\mathrm{d}\theta\int_0^{r_M} r\,\mathrm{d}r\,\mathbf{s}(r,\,\theta)\cdot\frac{\hat{\mathbf{r}}}{2\pi r}$$

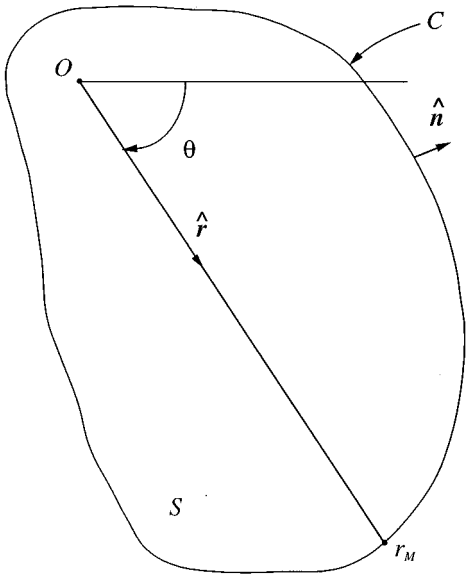

Fig. 2. Relevance of the use of Green's first identity in polar coordinates.

$$= \frac{1}{2\pi}\int_0^{2\pi} d\theta \phi(r_M, \theta) - \frac{1}{2\pi}\int_0^{2\pi} d\theta \int_0^{r_M} dr \mathbf{s}(r, \theta)\cdot\hat{\mathbf{r}} = \frac{1}{2\pi}\int_0^{2\pi} d\theta\left[\phi(r_M, \theta) + \int_{r_M}^{0} dr \mathbf{s}(r, \theta)\cdot\hat{\mathbf{r}}\right], \quad r_M \in C, \tag{7}$$

where the origin of coordinates has been set at the retrieved phase point $\mathbf{r}' = 0$, and $|\mathbf{r}' - \mathbf{r}| = r$ and $r_M = r_M(\theta)$; see also Fig. 2.

Interpretation of Eq. (7) is now in order. The phase value at $\mathbf{r}' = 0$ is the mean value of the line integrals over all the radial paths in any direction θ (Fig. 2). As a matter of fact, the integral inside the brackets represents the line integral on a straight path connecting point $\mathbf{r}' = 0$ (where we want to evaluate the phase) to the boundary along a fixed direction θ; $\phi(r_M, \theta)$ is the value on the border taken as the initial value of the phase; and the outer integral computes the mean value of the inner expression, which is θ dependent.

In absence of any corrupted region, all the line integrals generate the same value. In fact, in this case $\mathbf{s}$ is an irrotational field, and thus line integrals are independent of paths: they can be calculated from the values that the phase assumes on the boundary points of the integration interval:

$$\phi(0) = \frac{1}{2\pi}\int_0^{2\pi} d\theta[\phi(r_M) + \phi(0) - \phi(r_M)]. \tag{8}$$

Accordingly, the average coincides with the value that we would obtain by evaluating only one line integral (local integration).

3. FURTHER EXTENSION OF THE CONNECTION BETWEEN LOCAL AND GLOBAL TECHNIQUES

A particularly relevant case in most applications is represented by a rectangular domain of investigation. In this case it is useful to perform a periodization step to improve the computational efficiency of the phase-unwrapping methods,[9,12] which leads to procedures carried out by means of circular convolutions instead of linear ones. In Ref. 12 the extension of the Green's function method to periodic phase patterns was presented. In the rectangular domain $S = [-a/2, a/2[\times [-b/2, b/2[$ the periodic counterpart of Eq. (3) is[12]

$$\tilde{\phi}(x', y') = -\iint_S dS \tilde{\mathbf{s}}(x, y)\cdot\nabla\tilde{g}(x' - x, y' - y), \tag{9}$$

where $\tilde{\phi}$ and $\tilde{\mathbf{s}}$ are the periodic counterparts of ϕ and $\mathbf{s}$, respectively, and $\tilde{g}$ is Green's function for the periodic case, i.e., the solution of[12]

$$\nabla^2\tilde{g}(x, y) = \sum_{p,q=-\infty}^{+\infty} \delta(x - pa, y - qb). \tag{10}$$

Hence from Eq. (4),

$$\tilde{g}(x, y) = \sum_{p,q=-\infty}^{+\infty} g(x - pa, y - qb) = \mathrm{rep}_{a,b}[g(x, y)], \tag{11}$$

where the operator $\mathrm{rep}_{a,b}(\,)$ accounts for the summation of all the shifted replicas (by a and b spatial periods) of the considered function.

We now show that the global procedure is equivalent to averaging local integrations in this case, too. Inserting Eq. (11) into Eq. (9) leads to

$$\tilde{\phi}(x', y') = -\int_{-a/2}^{a/2} dx \int_{-b/2}^{b/2} dy\left[\tilde{\mathbf{s}}(x, y)\cdot\sum_{p,q=-\infty}^{+\infty}\nabla g(x' - x - pa, y' - y - qb)\right]. \tag{12}$$

With the substitutions $x + pa \to x$ and $y + qb \to y$, we have, further,

$$\begin{aligned}\tilde{\phi}(x', y') &= -\sum_{p,q=-\infty}^{+\infty}\int_{-a/2+pa}^{a/2+pa} dx \int_{-b/2+qb}^{b/2+qb} dy[\tilde{\mathbf{s}}(x - pa, y - qb)\cdot\nabla g(x' - x, y' - y)] \\ &= -\sum_{p,q=-\infty}^{+\infty}\int_{-a/2+pa}^{a/2+pa} dx \int_{-b/2+qb}^{b/2+qb} dy[\tilde{\mathbf{s}}(x, y)\cdot\nabla g(x' - x, y' - y)] \\ &= -\int_{-\infty}^{+\infty} dx \int_{-\infty}^{+\infty} dy[\tilde{\mathbf{s}}(x, y)\cdot\nabla g(x' - x, y' - y)],\end{aligned} \tag{13}$$

where the unbounded integral is intended as a summation of infinite integrals, each of them extended to the basic period, and we have used the equation

$$\tilde{\mathbf{s}}(x + pa, y + qb) = \tilde{\mathbf{s}}(x, y). \tag{14}$$

We again use polar coordinates for evaluating Eq. (13):

$$\tilde{\phi}(0) = -\int_0^{2\pi} \mathrm{d}\theta \int_0^{+\infty} r\,\mathrm{d}r\,\tilde{\mathbf{s}}(r, \theta)\,\frac{\hat{\mathbf{r}}}{2\pi r}$$

$$= \frac{1}{2\pi}\int_0^{2\pi} \mathrm{d}\theta \left[\int_{+\infty}^{0} \mathrm{d}r\,\tilde{\mathbf{s}}(r, \theta)\cdot\hat{\mathbf{r}}\right]. \tag{15}$$

where the origin of the coordinates has been set at the retrieved phase point $\mathbf{r}' = 0$, and $|\mathbf{r}' - \mathbf{r}| = r$, just as it is in the nonperiodic case. Equation (15) clearly shows that, also in the case at hand, the phase value at $\mathbf{r}' = 0$ is the mean value of line integrals over all the radial paths along any direction θ; in this case, however, the integrals extend to infinity. Note that the periodization step eliminates the contribution of the phase values on the border, as one can see by comparing Eqs. (15) and (7), but introduces impulsive outward components of $\nabla\tilde{\phi}$ on the border of each basic period, which cannot be directly evaluated from the wrapped data.[12] We must account for these impulsive components in the calculation of Eq. (9), since the portion of the boundary represented by the following parametric equations,

$$\begin{cases} x = -a/2, \\ y = t, \qquad t \in [-b/2, b/2[, \end{cases}$$

$$\begin{cases} x = t, \qquad t \in [-a/2, a/2[, \\ y = -b/2, \end{cases} \tag{16}$$

is included in the integration domain S (further details on this topic can be found in Ref. 12).

Different solutions to overcome this lack of information have been proposed in the literature. In Ref. 12 it was shown that one can estimate the unknown impulsive components of the gradient by iteratively solving a Fredholm equation of second kind, similarly to the non-periodic case. A different solution, which avoids this estimation step, is referred to as the mirror reflection approach[9] and is carried out on the measured phase before the periodization; then the resulting gradient does not exhibit any impulsive components on the border. The trade-off for this result is a 4× increase in the amount of data to be processed. The two methods have also been demonstrated to be equivalent.[12]

4. WEIGHTED CASE

Let us focus on weighted global algorithms and show that the analysis done in Section 2 can be extended to this case. Weighted LS algorithms are based on the minimization of the following functional[5,8]:

$$\|w\nabla\phi - w\mathbf{s}\|^2 = \min, \tag{17}$$

where $w(x, y)$ is a weighting function set to 0 in the region to be excluded (weighted areas) and to 1 elsewhere. The solution to this problem is generally performed by means of iterative procedures.[5,8] An alternative solution to Eq. (17) is considered in the following. It basically corresponds to a global integration operation on a multiconnected domain instead of on a single connected one, where the additional boundaries are generated by the excluded corrupted regions. A pictorial example is given in Fig. 3. In this case Eq. (3) is still valid, but we have to add the additional boundary contour $C_1 = C^+ + C^-$ (see Fig. 3):

$$\phi(\mathbf{r}') = -\iint_{S-W} \mathrm{d}S\,\mathbf{s}(\mathbf{r})\cdot\nabla g(\mathbf{r}' - \mathbf{r}) + \oint_C \mathrm{d}c\,\phi(\mathbf{r}_C)\,\frac{\partial g(\mathbf{r}' - \mathbf{r}_C)}{\partial n} + \oint_{C_1} \mathrm{d}c\,\phi(\mathbf{r}_C)\,\frac{\partial g(\mathbf{r}' - \mathbf{r}_C)}{\partial n}, \qquad \mathbf{r}' \in S, \tag{18}$$

where C_1 consists of a close line around the weighed zone W. Using polar coordinates again, we now have

$$\phi(0) = \phi_{2\pi-\Delta\alpha}(0) + \frac{1}{2\pi}\int_{\Delta\alpha} \mathrm{d}\theta \left[\int_{r_M}^{r_{C^+}} \mathrm{d}r\,\mathbf{s}(r, \theta)\cdot\hat{\mathbf{r}} + \int_{r_{C^-}}^{0} \mathrm{d}r\,\mathbf{s}(r, \theta)\cdot\hat{\mathbf{r}}\right] - \frac{1}{2\pi}\int_{\Delta\alpha} \mathrm{d}\theta\,\phi(r_{C^+}, \theta) + \frac{1}{2\pi}\int_{\Delta\alpha} \mathrm{d}\theta\,\phi(r_{C^-}, \theta) + \frac{1}{2\pi}\int_{\Delta\alpha} \mathrm{d}\theta\,\phi(r_M, \theta). \tag{19}$$

where $\phi_{2\pi-\Delta\alpha}(0)$ can be evaluated by Eq. (7) applied to all points not included in the angular sector $\Delta\alpha$. After some mathematical manipulations, Eq. (19) can be recast in the following form:

$$\phi(0) = \phi_{2\pi-\Delta\alpha}(0) + \frac{1}{2\pi}\int_{\Delta\alpha} \mathrm{d}\theta \left\{\phi(r_M, \theta) + \int_{r_M}^{r_{C^+}} \mathrm{d}r\,\mathbf{s}(r, \theta)\cdot\hat{\mathbf{r}} + [\phi(r_{C^-}, \theta) - \phi(r_{C^+}, \theta)] + \int_{r_{C^-}}^{0} \mathrm{d}r\,\mathbf{s}(r, \theta)\cdot\hat{\mathbf{r}}\right\}. \tag{20}$$

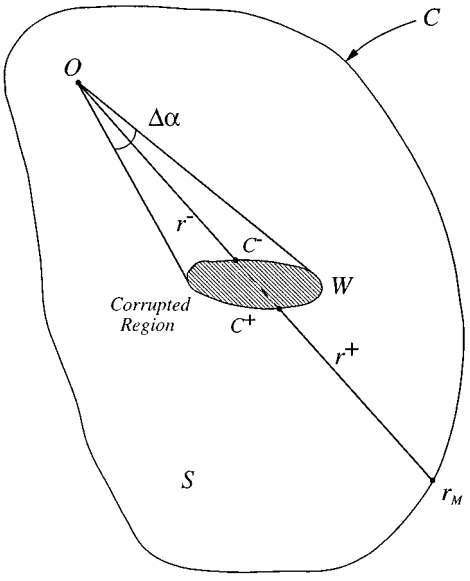

Fig. 3. Multiconnected domain.

Interpretation of Eq. (20) is now in order. Let us consider, for a fixed angle θ, the terms inside the braces. The first term is the initial value; the second accounts for the integration of **s** along the radial path from the outer contour to the inner one; the third term is the phase jump across the excluded area and replaces the integral within the weighted area where the gradient is incorrectly estimated; the fourth term is the integration of **s** over the remaining path. The outer integral represents the mean operation (over the angular sector $\Delta\alpha$) of the summation of the above-mentioned path-following integrals. Accordingly, in the weighted case also, the global procedure is equivalent to averaging the results of local integration over all radial paths.

A comment is now in order. If we exclude from the integration all the areas where **s** is incorrectly estimated and we have the correct value of the phase on the boundaries, the expression in braces in Eq. (20) provides the correct value for the unwrapped phase. However, if all the corrupted regions could be detected, it would not make any sense to apply Eq. (20) instead of the local integration and branch-cut approach, which is certainly simpler to implement and achieves better computational efficiency. In practical cases it is not always possible to detect and exclude all the corrupted regions (in particular, in the case of interferometric synthetic-aperture radar[3]); thus a global weighted approach, like that of Eq. (20), is then more convenient because the error derived from these undetected areas is reduced by the mean operation. In this sense we can state that the global procedures are more robust than the local ones. An interpretation of the effect of undetected corrupted regions is given in Section 5.

5. EFFECT OF UNDETECTED CORRUPTED REGIONS ON PHASE-UNWRAPPING TECHNIQUES

Let us now analyze the effect of nonexcluded corrupted regions on the unwrapped phase pattern; since we have already shown the relationship between local and global algorithms, the overall analysis is done in terms of path-following integration.

We model the undetected corrupted region as a phase discontinuity located along a line parallel to the x axis (Fig. 4);

$$\nabla\phi = \mathbf{s} + 2\pi N\delta(y - y_0)\mathrm{rect}\left(\frac{x - x_0}{2L}\right)\hat{\mathbf{y}}. \tag{21}$$

Accordingly, the recovered phase value $\hat{\phi}(x, y)$ is an incorrect reconstruction of the true phase $\phi(x, y)$. The phase error is given by

$$\epsilon(x, y) = \phi(x, y) - \hat{\phi}(x, y). \tag{22}$$

In the case of local integration we have

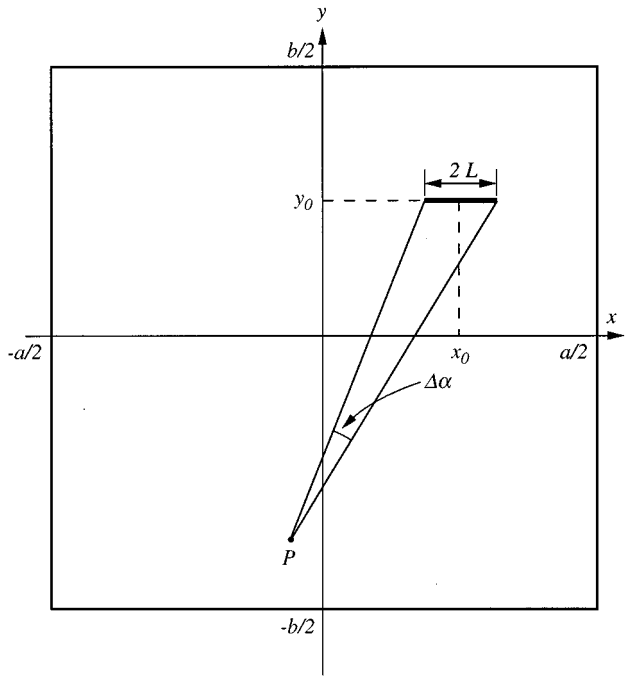

Fig. 4. Relevance of error propagation resulting from a line of phase discontinuity.

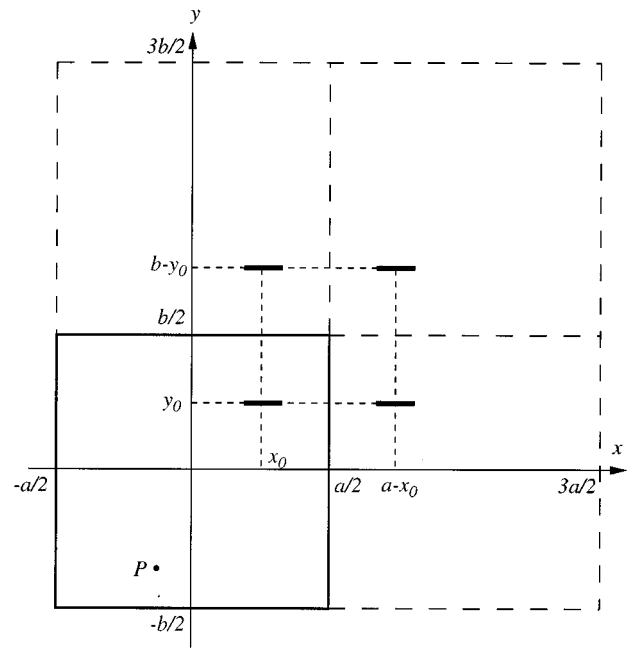

Fig. 5. Mirrored domain.

$$\epsilon(x, y) = \phi(x, y) - \int_{P_0}^{P(x, y)} \mathrm{d}c\,\mathbf{s}\cdot\hat{\mathbf{c}}$$

$$= 2\pi N\int_{P_0}^{P(x, y)} \mathrm{d}c\,\delta(y - y_0)$$

$$\times\ \mathrm{rect}\left(\frac{x - x_0}{2L}\right)\hat{\mathbf{y}}\cdot\hat{\mathbf{c}}, \tag{23}$$

which is path dependent; thus the form of the error depends on the integration path and on its relative position to the corrupted region.

Let us now concentrate on the global integration approach. In this case, all the paths that connect the border to point P and are not included in the angular sector $\Delta\alpha$ provide the correct unwrapped phase value at point P, thus leading to zero error (see Fig. 4). In contrast, each path that crosses the undersampled area (i.e., the area included in angular sector $\Delta\alpha$) gives rise to an error at point P whose amplitude is $2\pi N$. If we know the unwrapped phase on the border, it follows from Eq. (7) that the total error is proportional to the amplitude of angular sector $\Delta\alpha$ divided by 2π (Ref. 10):

$$\epsilon(x, y) = N\Delta\alpha(x, y). \tag{24}$$

Accordingly, the error decreases at least as much as the inverse of the distance of the observation point from the undersampled area. Note also that the sign of this error depends on the relative position between observation point P and the location of the undersampled area; in fact, that sign depends on $\hat{\mathbf{y}} \cdot \hat{\mathbf{r}}$ [see Eq. (7)] where $\hat{\mathbf{y}}$ is a unit vector pointing in the direction of the undesired component of the gradient in Eq. (21).

The effect of periodization and mirror reflection (which are used in practical cases) is now briefly investigated. The domain shown in Fig. 4 maps, in this case, onto that of Fig. 5 as a result of the mirror reflection operation, and the periodic mirrored version of Eq. (21) is

$$\begin{aligned}\nabla\tilde{\phi} = \tilde{\mathbf{s}} + \mathrm{rep}_{2a,2b}\Bigg\{ 2\pi N\Bigg[&\delta(y - y_0)\mathrm{rect}\left(\frac{x - x_0}{2L}\right) \\ &+ \delta(y - y_0)\mathrm{rect}\left(\frac{a - x - x_0}{2L}\right) \\ &+ \delta(b - y - y_0)\mathrm{rect}\left(\frac{x - x_0}{2L}\right) \\ &+ \delta(b - y - y_0)\mathrm{rect}\left(\frac{a - x - x_0}{2L}\right)\Bigg]\hat{\mathbf{y}}\Bigg\}. \end{aligned} \tag{25}$$

As already stated,[12] no boundary estimation is necessary after the mirror reflection; hence we can use Eq. (15) to compute the induced error at observation point P. The mirrored, undesired error contributions to the gradient in Eq. (25) give rise to the mirrored version of the error in Eq. (24) on the recovered phase. Thus, by superimposition, we have

$$\begin{aligned}\tilde{\epsilon}(x, y) = &\ \mathrm{rep}_{2a,2b}[N\Delta\alpha(x, y)] \\ &+ \mathrm{rep}_{2a,2b}[N\Delta\alpha(a - x, y)] \\ &+ \mathrm{rep}_{2a,2b}[N\Delta\alpha(x, b - y)] \\ &+ \mathrm{rep}_{2a,2b}[N\Delta\alpha(a - x, b - y)]. \end{aligned} \tag{26}$$

Note that the convergence of the four series in Eq. (26) is guaranteed by the fact that for a fixed observation point P, the terms of the series decrease; furthermore, they have alternate signs because of the relative position of the replicated undersampled area with respect to P. Comparison of Eqs. (24) and (26) shows the change in the form of the error.

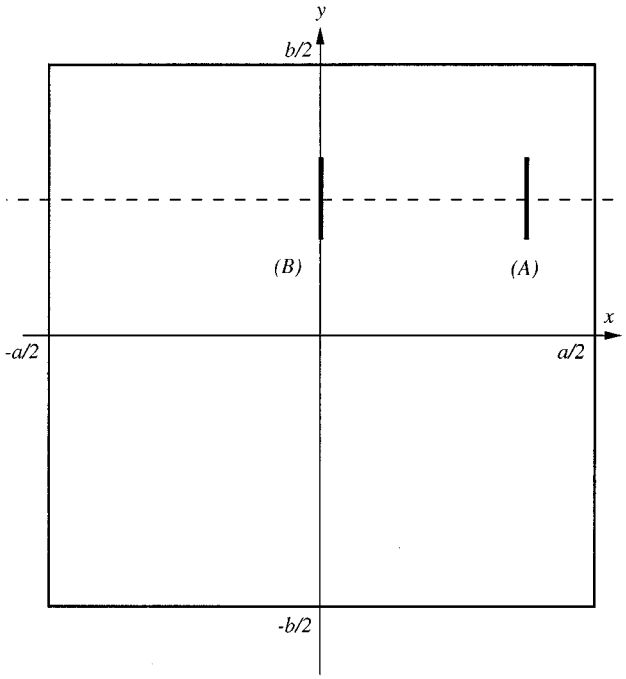

Fig. 6. Relevance of a rectangular domain with different locations, (A) and (B), of a corrupted region.

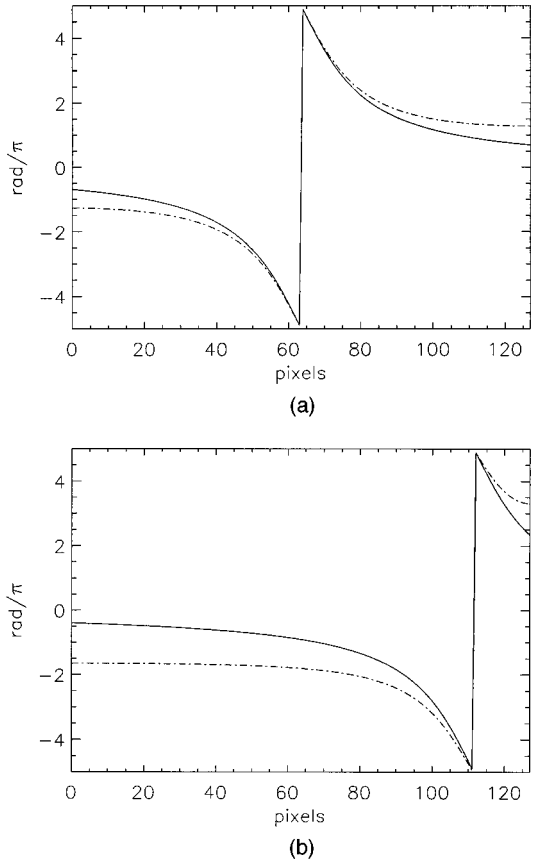

Fig. 7. Error functions obtained in presence (solid curves) and in the absence (dashed–dotted curves) of boundary information for the corrupted region. (a) Case (A) of Fig. 6, (b) case (B) of Fig. 6. The phase jump is 10π rad.

As a consequence of Eq. (26) we note that the location (with respect to the boundaries) of the corrupted area plays an important role in the overall error. To highlight this point we consider cases (A) and (B) depicted in Fig. 6. Case (A) corresponds to a corrupted region near the boundaries, whereas in (B) the undersampled area is far from one of the boundaries. For both cases we computed the error functions along the horizontal dashed line in Fig. 6; error functions are shown for case (A) in Fig. 7(a) and for case (B) in Fig. 7(b). In both figures the solid curves represent the result of Eq. (24). The dashed–dotted curves represent the application of the mirror reflection (to get rid of the necessity for phase information on the boundaries) that results from Eq. (26). Examination of Figs. 7(a) and 7(b) shows that in the former case (solid curves) the error spread is independent of the corrupted region's location, whereas in the latter case (dashed–dotted curves) the error depends on the corrupted region's location.

6. CONCLUSIONS

We have proved that both local and global integrations are based on line integration of the phase-gradient estimate. In the first case the obtained value is either right or wrong, depending on the choice of integration path. In the second case the value is obtained by averaging the results of all radial paths.

An interpretation of the weighted global unwrapping procedure in terms of local integration has also been given. In this case we have shown that the averaging operation characterizing the global approach does not involve that part of the paths that crosses the weighted areas. However, the original phase must be known or estimated on the additional boundaries around the weighted areas.

Finally, we have discussed the effect of nonexcluded corrupted regions on the unwrapped phase in terms of path-following integration. As a consequence we have shown that nonexcluded corrupted regions cause errors, depending on their location, not only for local but for global algorithms as well.

ACKNOWLEDGMENTS

This study was partially supported by Alenia Spazio S.p.A., Rome, and by the Italian Space Agency. We thank the anonymous reviewers for their valuable comments. We also thank John Corvino for proofreading the manuscript.

REFERENCES

1. R. H. Hudgin, "Wave-front reconstruction for compensated imaging," J. Opt. Soc. Am. A **67**, 370–375 (1977).
2. H. A. Zebker and R. M. Goldstein, "Topographic mapping from interferometric synthetic aperture radar observations," J. Geophys. Res. **91**, 4993–4999 (1986).
3. Q. Lin, F. Vesecky, and H. A. Zebker, "Comparison of elevation derived from INSAR data with DEM over large relief terrain," Int. J. Remote Sensing **15**, 1775–1790 (1994).
4. R. M. Goldenstein, H. A. Zebker, and C. L. Werner, "Satellite radar interferometry: two-dimensional phase unwrapping," Radio Sci. **23**, 713–720 (1988).
5. G. Fornaro, G. Franceschetti, R. Lanari, D. Rossi, and M. Tesauro, "Finite element method for interferometric SAR phase unwrapping," presented at the EUROPTO '96 meeting, Taormina, Italy, September 23–26, 1996.
6. H. Takajo and T. Takahashi, "Noniterative methods for obtaining the exact solution for the normal equation in least-squares phase estimation from phase difference," J. Opt. Soc. Am. A **5**, 1818–1827 (1988).
7. D. C. Ghiglia and L. A. Romero, "Direct phase estimation from phase difference using fast elliptic partial differential equation solvers," Opt. Lett. **14**, 1107–1109 (1989).
8. D. C. Ghiglia and L. A. Romero, "Robust two-dimensional weighted and unweighted phase unwrapping that uses fast transform and iterative methods," J. Opt. Soc. Am. A **11**, 107–117 (1994).
9. M. D. Pritt and J. S. Shipman, "Least-squares two dimensional phase unwrapping using FFT's," IEEE Trans. Geosci. Remote Sensing **32**, 706–708 (1994).
10. G. Fornaro, G. Franceschetti, and R. Lanari, "Interferometric SAR phase unwrapping using Green's formulation," IEEE Trans. Geosci. Remote Sensing **34**, 720–727 (1996).
11. U. Spagnolini, "2-D Phase unwrapping and instantaneous frequency estimation," IEEE Trans. Geosci. Remote Sensing **33**, 579–589 (1995).
12. G. Fornaro, G. Franceschetti, R. Lanari, and E. Sansosti, "Robust phase unwrapping techniques: a comparison," J. Opt. Soc. Am. A **13**, 2355–2366 (1996).
13. C. Prati, M. Giani, and N. Leuratti, "SAR Interferometry: a 2-D phase unwrapping technique based on phase and absolute values information," presented at the International Geoscience and Remote Sensing Symposium (IGARSS) '90, Washington, D.C., May 20–24, 1990.
14. W. Xu and I. Cumming, "A region growing algorithm for InSAR phase unwrapping," presented at the International Geoscience and Remote Sensing Symposium (IGARSS) '96, Lincoln, Nebr., May 27–31, 1996.
15. M. D. Pritt, "Phase unwrapping by means of multigrid techniques for interferometric SAR," IEEE Trans. Geosci. Remote Sensing **34**, 728–738 (1996).
16. D. J. Bone, "Fourier fringe analysis: the two-dimensional phase unwrapping problem," Appl. Opt. **30**, 3627–3632 (1991).
17. R. Cusak, J. M. Huntley, and H. T. Goldrein, "Improved noise-immune phase-unwrapping algorithm," Appl. Opt. **34**, 781–789 (1995).
18. J. A. Quiroga, A. Gonzàlez-Cano, and E. Bernabeu, "Stable-marriages algorithms for preprocessing phase maps with discontinuity sources," Appl. Opt. **34**, 5029–5038 (1995).
19. J. R. Buckland, J. M. Huntley, and S. R. E. Turner, "Unwrapping noisy phase maps by use of a minimum-cost-matching algorithm," Appl. Opt. **34**, 5100–5108 (1995).
20. N. H. Ching, D. Rosenfeld, and M. Braun, "Two-dimensional phase unwrapping algorithm using a minimum spanning tree algorithm," IEEE Trans. Image Process. **1**, 355–365 (1992).